Integrating Time-Frequency and Machine Learning Methods for Tracking In Radar and Communications Coexisting Systems

by

Yiming Zhang

A Thesis Presented in Partial Fulfillment
of the Requirement for the Degree
Master of Science

Approved April 2022 by the
Graduate Supervisory Committee:

Antonia Papandreou-Suppappola, Chair
Bahman Moraffah
Cihan Tepedelenlioglu

ARIZONA STATE UNIVERSITY

May 2022

ABSTRACT

Increased demand on bandwidth has resulted in wireless communications and radar systems sharing spectrum. As signal transmissions from both modalities coexist, methodologies must be designed to reduce the induced interference from each system. This work considers the problem of tracking an object using radar measurements embedded in noise and corrupted from transmissions of multiple communications users. Radar received signals in low noise can be successively processed to estimate object parameters maximum likelihood estimation. For linear frequency-modulated (LFM) signals, such estimates can be efficiently computed by integrating the Wigner distribution along lines in the time-frequency (TF) plane. However, the presence of communications interference highly reduces estimation performance.

This thesis proposes a new approach to increase radar estimation performance by integrating a highly-localized TF method with data clustering. The received signal is first decomposed into highly localized Gaussians using the iterative matching pursuit decomposition (MPD). As the MPD is iterative, high noise levels can be reduced by appropriately selecting the algorithm's stopping criteria. The decomposition also provides feature vectors of reduced dimensionality that can be used for clustering using a Gaussian mixture model (GMM). The proposed estimation method integrates along lines of a modified Wigner distribution of the Gaussian clusters in the TF plane. Using simulations, the object parameter estimation performance of the MPD is shown to highly improve when the MPD is integrated with GMM clustering.

ACKNOWLEDGEMENTS

The work presented in this thesis is the result from years of unyielding focus and dedication that was made possible through various sources of motivation and support. I would be remiss if I failed to acknowledge the individuals whom have been there for help and guidance when I needed it the most.

First, I would like to thank my advisor Prof. Antonia Papandreou-Suppappola who has provided mentoring, support, and guidance for both professional and personal purposes on an uncountable number of situations. All of this will not happen if she did not invite me to the lab, and I am very lucky to meet the coolest professor in the world.

My sincerest thanks to my mother, father. None of this would have been possible without their patience for understanding the challenges that I had to overcome as well as their motivation, guidance, emotional and financial support. I am forever grateful for their enduring help.

More importantly, I would like to give special thanks to my girlfriend Huanhuan Zou for her love, understanding, continuing support in both physical and mental ways when undertaking my research and writing my thesis. Your gentle encouragement for me was what sustained me this far.

Lastly, I would like to thank all of the members of the Signal Processing and Adaptive Sensing laboratory for sharing materials and providing useful research discussions.

TABLE OF CONTENTS

Page

CHAPTER Page

LIST OF TABLES

LIST OF FIGURES

Chapter 1

INTRODUCTION

1.1 Motivation and Introduction

1.1.1 Radar and Communications Coexistence

Spectrum sharing between multiple sensing modalities is becoming a necessity as advances in technology require increasingly more resources for operation [2, 3, 4, 5, 6]. In wireless communications, higher bandwidths are needed to allow for higher rates of data transfer. In radar, there is an increased need of reliable capabilities, especially for monitoring and security. Under normal operation, radar and communications systems are allocated unique spectral bands and must follow established spectrum allocation regulations by the International Telecommunication Union (ITU) [7, 8]. Due to the increased demand on the finite amount of spectrum as well as the physical constraints required to stay within a specific spectrum band, systems are now faced with the problem of spectrum congestion. Currently, spectrum congestion has affected weather radars [9], airport surveillance radars [10] and remote sensing systems [11]. In radar and communications systems, it has become necessary to develop methods for processing both systems while sharing the same frequency band [12, 13, 14, 15, 16, 17, 18, 19, 20, 21, 22, 23]. For example, both target position and user communication messages must be estimated in a system with both

radar and wireless communication modalities. One approach to sharing spectrum is the design of transmit waveforms for both systems [24, 25, 26, 27, 28, 22, 29, 30, 31, 32]. Another approach to sharing spectrum is for one system to design methods to reduce the interference caused by the other system [11, 33, 34, 35, 36, 37]. From the radar receiver perspective, signals from multiple communication users are perceived as interference in the shared spectrum. Radar processing thus requires advanced processing methods to improve radar performance as both noise and interference need to be reduced.

1.1.2 Advanced Signal Processing Methodologies

Time-frequency representations (TFRs) are two-dimensional (2-D) signal transformations for analyzing time-varying signals, that is, signals whose frequency content changes with time [38, 39, 40]. Such signals can be found in many applications, including radar and wireless communications. The Wigner distribution (WD) is a well-known TFR as it satisfies many desirable signal properties, including preservation of the signal's time shifts, frequency shifts and scale changes [38, 39]. For successful analysis, it is important to match a TFR to the signal's time-frequency (TF) structure. For example, the WD is ideally matched to linear frequency-modulated (LFM) signals as it provides a highly localized TF representation along the LFM's linear instantaneous frequency. Note, however, that the WD is a quadratic TFR, and as such, it suffers from cross term when used to analyze multicomponent signals [39].

The matching pursuit decomposition (MPD) based TFR also provides highly localized representation in the TF domain and in addition, it does not suffer from cross terms

[41, 42, 43]. The MPD is an iterative algorithm that decomposes an analysis signal into a weighted linear combination of Gaussian signals [41]. The Gaussian signals are selected from a predefined dictionary of time-shifted, frequency-shifted and scaled versions of a basic Gaussian atom. When a signal is decomposed using the MPD, each extracted atom is characterized by a vector of unique parameters, consisting of the TF shift, scale parameter and also weight coefficient. These vectors provide reduced dimensionality unique features for the analysis signal. The features can then be directly used with machine learning methods to provide unknown signal information.

1.2 Proposed Thesis Work

We consider the problem of tracking an object using measurements from a radar sensor that coexists with a multiple user communications system. At the detection stage, if prior information on the noise and communication interference is assumed known, the generalized Neyman-Pearson likelihood ratio test can be used to detect the radar echo return. As the method requires the maximum likelihood estimate (MLE) of the object parameters, it is not optimal in the sense of maximizing the probability of detection for a given probability of false alarm. However, it has been shown to work well in low noise environments. If an LFM signal is used, the MLE of its parameters can be found by integrating the WD TFR of the received signal over varying lines in the TF plane, corresponding to the signal's instantaneous frequency. However, in realistic scenarios, both noise and interference parameters must also be estimated, resulting in reduced detection performance.

This work proposes a method for increasing radar tracking performance by integrating a TF advanced signal processing method with a data clustering approach. We assume an LFM transmit signal for the radar and a frequency-modulation signaling scheme for the communications system. At the radar receiver, the overall noisy received signal is first represented as a weighted linear combination of Gaussian elementary atoms using the MPD. As the MPD is iterative, we select its stopping criterion to depend on the signal's residual energy in order to help reduce the overall noise in the received signal. The MPD extracted features can be used as input to a Gaussian mixture model (GMM) for clustering. With the limited information provided to the GMM algorithm, we do not expect the various mixture components to be clustered separately. Instead, we exploit the MPD TFR of the Gaussian atoms in each cluster. The TFR is formed as a weighted linear combination of the WD of the Gaussian atoms and the estimated parameters are found by integrating along TF lines.

1.3 Thesis Organization

The rest of this thesis is organized as follows. In Chapter 2, we provide background information on maximum likelihood estimation, matching pursuit decomposition, and Gaussian mixture modeling. In Chapter 3, we propose our method for estimating the position of an object in the presence of strong communications interference by integrating time-frequency signal processing and machine learning methods. In Chapter 4, we provide simulations to compare and demonstrate the improved estimation performance of our approach.

Chapter 2

BACKGROUND

2.1 Maximum Likelihood Estimation

In radar tracking applications, the aim is to estimate the parameters of an object. If the object is stationary, and the unknown parameters do not change with time, a commonly used estimation method is maximum likelihood estimation [44]. The maximum likelihood estimator (MLE) is unbiased and its variance can be shown to approach the Cramer-Rao lower bound (CRLB) for high signal-to-noise ratio (SNR) conditions or for large data records. Thus, the MLE provides an asymptotically efficient estimator [44]. By design, the MLE maximizes the likelihood function probability density function (PDF) $p(\mathbf{x};\theta)$ of a given measurement vector $\mathbf{x}$ with unknown parameter θ. Although in some cases the maximization results in closed form estimations, in most cases, the MLE estimate is obtained as

$$\theta_{\text{MLE}} = \hat{\theta} = \arg\max_{\theta \in S_\theta} p(\mathbf{x};\theta)$$

where S_θ is the set of all possible values of θ. The MLE method is demonstrated by the following examples.

2.1.1 MLE of Signal Aplitude

We first consider the example of finding the MLE of the deterministic and unknown amplitude parameter A [44]. The received signal samples are given by

$$x[n] = A + w[n], \;\; n = 0, \ldots, N-1,$$

where $w[n] \sim \mathcal{N}(0, \sigma^2)$ is zero-mean white Gaussian noise with variance σ^2. The MLE of A is found by maximizing the likelihood function,

$$A_{\text{MLE}} = \hat{A} = \arg\max_{A>0} p(\mathbf{x}; A)$$

The maximum value is obtained by solving

$$\frac{\partial}{\partial A} \ln\left(p(\mathbf{x}; A)\right) = 0\,.$$

Computing the derivative,

$$\begin{aligned}
\frac{\partial}{\partial A} \ln\left(p(\mathbf{x}; A)\right) &= \frac{\partial}{\partial A}\left(-\frac{1}{2\sigma^2}\sum_{n=0}^{N-1}(x[n]-A)^2\right) \\
&= \frac{1}{\sigma^2}\sum_{n=0}^{N-1}(x[n]-A) = \frac{1}{\sigma^2}\sum_{n=0}^{N-1}x[n] - \frac{N\,A}{\sigma^2} = 0 \\
\Rightarrow \;\; A_{\text{MLE}} &= \hat{A} = \frac{1}{N}\sum_{n=0}^{N-1}x[n] = \mathbf{x}
\end{aligned}$$

Thus, the MLE corresponds to the sample mean. It can be shown that this estimate is unbiased and efficient as it attains the CRLB.

2.1.2 MLE of Signal Time Delay

We consider the problem of estimating the time-delay χ of the transmit signal samples $s[n]$. The received signal samples are given by

$$x[n] = s[n-\chi] + w[n] = \cos\left(2\pi\beta\,(n-\chi)^2\right) + w[n],\ n = 0, \ldots, N-1 \qquad (2.1)$$

where $s[n] = \cos\left(2\pi\beta\, n^2\right)$ is a real linear frequency-modulated (LFM) signal with frequency modulation (FM) rate β, and $w[n] \sim \mathcal{N}(0, \sigma^2)$ is zero-mean white Gaussian noise with assumed known variance σ^2. The estimation process requires the PDF $p(\mathbf{x})$ of the $N \times 1$ received radar signal vector $\mathbf{x} = [x[0]\ x[1]\ \ldots\ x[N-1]]^T$. From Equation (3.4), the PDF of $\mathbf{x}$ depends on the PDF of the Gaussian noise vector $\mathbf{w} = [w[0]\ w[1]\ \ldots\ w[N-1]]^T$, which is given by

$$p(\mathbf{w}) = \frac{1}{(2\pi\sigma^2)^{N/2}} \exp\Big(-\frac{1}{2\,\sigma^2}\sum_{n=0}^{N-1} w^2[n]\Big)$$

As the signal $s[n]$ is assumed deterministic, the PDF of $\mathbf{x}$ is also Gaussian. Thus, the samples $x[n]$ are distributed according to

$$x[n] \sim \mathcal{N}(0, \sigma^2),\ n = 0, \ldots, \chi - 1$$

$$x[n] \sim \mathcal{N}(\mu[n;\chi], \sigma^2),\ n = \chi, \ldots, \chi + M - 1$$

$$x[n] \sim \mathcal{N}(0, \sigma^2),\ n = \chi + M, \ldots, N-1$$

where $\mu[n;\chi] = \cos\left(2\pi\beta\,(n-\chi)^2\right)$. Note that we consider three independent sample segments of $x[n]$ as the transmitted signal $s[n]$ is only present over $M < N$ samples. The

overall PDF is given by

$$p(\mathbf{x};\chi) = p_1(\mathbf{x};\chi)\, p_2(\mathbf{x};\chi)\, p_3(\mathbf{x};\chi)$$

where

$$p_1(\mathbf{x}) = \frac{1}{(2\pi\sigma^2)^{M_1/2}}\, \exp\Big(-\frac{1}{2\,\sigma^2} \sum_{n=0}^{\chi-1} x^2[n] \Big)$$

$$p_2(\mathbf{x};\chi) = \frac{1}{(2\pi\sigma^2)^{M/2}}\, \exp\Big(-\frac{1}{2\,\sigma^2} \sum_{n=\chi}^{\chi+M-1} \Big(x[n] - s[n-\chi] \Big)^2 \Big) \tag{2.2}$$

$$p_3(\mathbf{x};\chi) = \frac{1}{(2\pi\sigma^2)^{M_2/2}}\, \exp\Big(-\frac{1}{2\,\sigma^2} \sum_{n=\chi+M}^{N-1} x^2[n] \Big)\,.$$

where $M_1 = \chi$ and $M_2 = N - M - \chi$. Note that we can also write the overall PDF as

$$p(\mathbf{x};\chi) = \frac{1}{(2\pi\sigma^2)^{N/2}}\, \exp\Big(-\frac{1}{2\,\sigma^2} \sum_{n=0}^{N-1} x^2[n] \Big)$$

$$\cdot \exp\Big(-\frac{1}{2\,\sigma^2} \sum_{n=\chi}^{\chi+M-1} \Big(x^2[n] - 2\,x[n]\,s[n-\chi] + s^2[n-\chi] \Big) \Big)\,. \tag{2.3}$$

The MLE of χ corresponds to the value of χ that maximizes the likelihood function $p(\mathbf{x};\chi)$ over all possible values of χ in the set $S_\chi = \{1, N - M + 1\}$. Specifically,

$$\hat{n}_0 = \arg \max_{\chi \in S_\chi} p(\mathbf{x};\chi)$$

The likelihood function $p(\mathbf{x};\chi)$ is given by the PDF in Equation (2.3). As the noise variance is assumed known, and using the PDF in Equation (2.2), then the MLE can be found by maximizing

$$\hat{n}_0 = \arg \max_{\chi \in S_\chi} p_2(\tilde{\mathbf{x}};\chi)$$

where

$$p_2(\mathbf{x};\chi) = \frac{1}{(2\pi\sigma^2)^{M/2}}\,\exp\Big(-\frac{1}{2\,\sigma^2}\sum_{n=\chi}^{\chi+M-1}\Big(x[n]-s[n-\chi]\Big)^2\Big)$$

$$= \frac{1}{(2\pi\sigma^2)^{M/2}}\,\exp\Big(-\frac{1}{2\,\sigma^2}\sum_{n=\chi}^{\chi+M-1}x^2[n]\Big)\exp\Big(-\frac{1}{2\,\sigma^2}\sum_{n=\chi}^{\chi+M-1}s^2[n-\chi)\Big)$$

$$\cdot\,\exp\Big(\frac{1}{2\,\sigma^2}\sum_{n=\chi}^{\chi+M-1}2x[n]\,s[n-\chi]\Big).$$

As the first two terms remain the same for any χ value, and also the energy of $s[n]$ is constant, irrespective of the time shift, then the MLE of χ can be as

$$\hat{n}_0 = \arg\,\max_{\chi\in S_\chi}\exp\Big(\frac{1}{\sigma^2}\sum_{n=\chi}^{\chi+M-1}x[n]\,s[n-\chi]\Big)$$

or, as the exponential function is monotonic,

$$\hat{n}_0 = \arg\,\max_{\chi\in S_\chi}\sum_{n=\chi}^{\chi+M-1}x[n]\,s[n-\chi] = \arg\,\max_{\chi\in S_\chi}2\,\mathbf{x}_\chi^T\mathbf{s}$$

where $\mathbf{x}_\chi = [x[\chi]\ x[\chi+1]\ \ldots\ x[\chi+M-1]]^T$ and $\mathbf{s} = [s[0]\ s[1]\ \ldots\ s[M-1]]^T$ are $M\times 1$ vectors, and $\mathbf{x}_\chi^T\mathbf{s} = \langle\mathbf{x}_\chi,\,\mathbf{s}\rangle$ can be computed as an inner product; here, $\mathbf{x}_\chi^T$ denotes the transpose of $\mathbf{x}_\chi$. We can also write the MLE as

$$\hat{n}_0 = \arg\,\max_{\chi\in S_\chi}\big(\langle\tilde{\mathbf{x}}_\chi,\,\mathbf{s}\rangle\big)^2$$

$$= \arg\,\max_{\chi\in S_\chi} = \sum_{n=\chi}^{\chi+M-1}\sum_{m=\chi}^{\chi+M-1}x[n]\,x[m]\,s[n-\chi]\,s[m-\chi] \tag{2.4}$$

$$\tag{2.5}$$

2.1.3 Computation of Time Delay MLE Using Time-frequency Methods

The Wigner distribution (WD) of a signal $s(t)$, defined as [45]

$$W_s(t,f) = \int_{-\infty}^{\infty} s\left(t+\frac{\tau}{2}\right)\, s^*\left(t-\frac{\tau}{2}\right)\, e^{-j2\pi\tau f}\, d\tau\,,$$

is a time-frequency representation (TFR) that is well matched to LFM signals. In particular, the WD of an LFM signal, assuming infinite duration, can be shown to be

$$s(t) = e^{j2\pi\alpha t^2} \;\overset{\text{WD}}{\longleftrightarrow}\; W_s(t,f) = \delta(f - 2\,\alpha\, t)\,. \tag{2.6}$$

Thus, the WD of the LFM signal is highly localized along the line $f = 2\alpha t$ in the time-frequency (TF) plane. This is a line with whose slope $2\,\alpha$ depends on the FM rate α. The WD also preserves time shifts on the analysis signal,

$$s(t-\tau) = e^{j2\pi\alpha(t-\tau)^2} \;\overset{\text{WD}}{\longleftrightarrow}\; W_z(t,f) = W_s(t-\tau,f)\,.$$

Applying this property to the LFM signal in Equation (2.6) results in

$$W_s(t-\tau,f) = \delta\Big(f - 2\,\alpha\,(t-\tau)\Big) = \delta\Big((f + 2\,\alpha\,\tau) - 2\,\alpha\, t\Big)\,.$$

Note that time shifting the LFM by τ is equivalent to frequency shifting the LFM by $-2\,\alpha\tau$.

The WD also preserves inner products as it satisfies Moyal's formula (or unitarity property). In particular, considering two continuous-time domain signals $x(t)$ and $z(t)$, then

$$\begin{aligned}(\langle\, \mathbf{x},\, \mathbf{z}\,\rangle)^2 &= \int\int x(t)\, z(t)\, x(t')\, z(t')\, dt'\, dt \\ &= \langle\langle\, W_x,\, W_z\,\rangle\rangle = \int_{-\infty}^{\infty}\int_{-\infty}^{\infty} W_x(t,f)\, W_z(t,f)\, dt\, df\,. \end{aligned} \tag{2.7}$$

If we replace $z(t)$ with the time-shifted LFM signal $s(t-\tau)$, and we use relation

$$\int_{-\infty}^{\infty} S(f)\,\delta(f-f_0)\,df = S(f_0)$$

then we can simplify Equation (2.7) to

$$(\langle\, \mathbf{x},\, \mathbf{z}\,\rangle)^2 = \int_{-\infty}^{\infty}\int_{-\infty}^{\infty} W_x(t,f)\,\delta\Big(f - 2\,\alpha\,(t-\tau)\Big)dtdf = \int_{-\infty}^{\infty} W_x(t, 2\,\alpha\,(t-\tau))dt \quad (2.8)$$

The relation in Equation (2.8) shows that computing the magnitude-squared fo the inner product of the time domain signals can simplify to integrating the WD along the line $f = 2\,\alpha\,(t-\tau)$. This is a useful result that we can use to obtain the MLE of the time shift of the LFM signal in Equation (2.5). For implementation, we need to compute Equation (2.8) using the discrete WD (DWD). For real part of the signals, the DWD is given by

$$W_x[n,k] = \sum_{m=-0}^{N-1} x[n+m]\,x^*[n-m]\,e^{-j2\pi mk/N},\;\; n,k = 0,\ldots,N-1\,.$$

provided that $n-m \in \{0,1,\ldots,N-1\}$ and $n+m \in \{0,1,\ldots,N-1\}$.

For the DWD, it can be shown that the unitarity property is given by

$$\Big(\sum_{n=0}^{N-1} x[n]\,s[n]\Big)^2 = \frac{1}{N}\sum_{n=0}^{N-1}\sum_{k=0}^{N-1} W_x[n,k]\,W_s[n,k] \quad (2.9)$$

The proof of Equation (2.9) is given in Appendix A. Using the DWD unitarity property and Equations (2.8), the MLE of the discrete time delay is given by

$$\hat{n}_0 = \arg\,\max_{\chi\in S_\chi}\;\frac{1}{N}\sum_{n=\chi}^{\chi+M-1} W_x[n, \lceil 2\,\beta\,(n-\chi)\rceil\,] \quad (2.10)$$

where the range of χ values is $S_\chi = \{1, N-M+1\}$. Thus, if Equation (3.7) is used instead of Equation (2.5), then the MLE computational cost is reduced. Instead of two

summations in Equation (2.5), Equation (3.7) only requires one summation. Specifically, the MLE of χ can be obtained simply by maximizing the sum of the WD values at discrete time-frequency points $[n, \lceil 2\,\beta\,(n-\chi)\rceil]$ for $n=0,\ldots,N-1$.

2.2 Matching Pursuit Decomposition

The matching pursuit decomposition (MPD) is an iterative algorithm that decomposes an analysis signal $x(t)$ into a weighted linear combination of atoms [41]. The atoms are selected from a complete and redundant dictionary using successive approximations of the signal with orthogonal projections on dictionary elements. In [41], a dictionary of Gaussian atoms with all possible TF shifts and scale changes, and a quadratic TFR was obtained by summing the Wigner distribution (WD) of each selected atom in the expansion. This modified WD is free of cross terms, and preserves signal energy, TF shifts, and scale changes [41, 42]. The MPD-based TFR, the modified WD (MWD) is defined that is highly localized for Gaussian signals in the TF domain [41, 42, 46]. Note that different MPD algorithms were also proposed to match signals with varying nonlinear TF characteristics [47, 48, 43].

The MPD dictionary is formed using a basic Gaussian signal $g(t) = e^{-t^2/2}$ as it is the most concentrated signal in TF, according to the uncertainty principle [38]. The dictionary $\mathcal{D}$ consists of time-shifted, frequency-shifted and scaled versions of the basic Gaussian

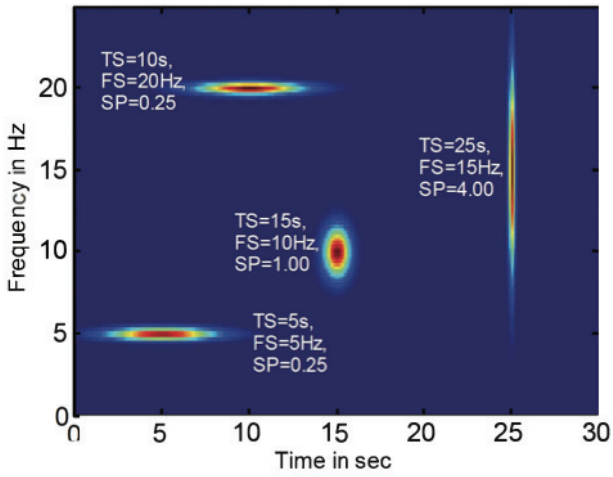

Figure 2.1: Example of Four Gaussian Atoms from the MPD Dictionary Using Different Time Shifts (TS), Frequency Shifts (FS) and Scales (SP). (Taken From [1])

signal

$$g_{\gamma_k}(t) = \sqrt{a_k}\; g(a_k(t-\tau_k)\, e^{j2\pi\nu_k t} = \sqrt{a_k}\;\exp\!\big(-a_k^2\,(t-\tau_k)^2/2\big)\;e^{j2\pi\nu_k t}$$

The parameter set of the kth dictionary atom is $\gamma_k = \{\tau_k,\ \nu_k,\ a_k\}$, $\gamma_k \in \Gamma$ where $\tau_k \in \mathbb{R}$ is time-shift, $\nu_k \in \mathbb{R}$ is frequency-shift and $a_k \in \mathbb{R}^+$ is scale parameter. Some example atoms in the MPD dictionary are shown in Figure 2.1.

We use the MPD to iteratively decompose a finite energy signal $x(t)$ as

$$x(t) = \sum_{i=0}^{\infty} \beta_i\; g_{\gamma_i}(t)$$

where $g_{\gamma_i}(t)$ and β_i is the ith selected dictionary atom and expansion coefficient, respectively. At the ith iteration, and starting with $r_0(t) = x(t)$, we form the inner product of the residual signal $r_i(t)$ and each dictionary element. We then select the ith element $g_{\gamma_i}(t)$ that

results in the maximum inner product. Specifically, we select $g_{\gamma_i}(t)$ such that

$$g_{\gamma_i}(t) = \arg \max_{g_\gamma \in \mathcal{D}} \left| \int_{-\infty}^{\infty} r_i(t)\, g_\gamma^*(t)\ \mathrm{d}t \right| = \arg \max_{g_\gamma \in \mathcal{D}} |\langle r_i, g_\gamma \rangle|$$

The residual signal is given by

$$r_{i+1}(t) = r_i(t) - \beta_i\, g_{\gamma_i}$$

where the ith expansion coefficient is given by

$$\beta_i = \int_{-\infty}^{\infty} r_i(t)\, g_{\gamma_i}^*(t)\ \mathrm{d}t$$

The signal representation up to the ith iteration is

$$x(t) = r_{i+1}(t) + \sum_{\ell=0}^{i} \beta_\ell\ g_{\gamma_\ell}(t)$$

The maximum number of iterations L is normally selected to ensure that $E\%$ of the signal energy has been extracted, where E is a pre-defined threshold. After L iterations, the signal can be represented as

$$x(t) = r_L(t) + \sum_{i=0}^{L-1} \beta_i\ g_{\gamma_i}(t)$$

A block diagram summarizing the MPD is given in Figure 2.2.

Note that the ith extracted Gaussian atom is characterized by the four-dimensional (4-D) feature vector $[\beta_i \ \ \tau_i \ \ \nu_i \ \ a_i]$, $i = 0, \ldots L-1$. Using these feature vectors, a highly localized TFR can be constructed as the weighted linear combination of the WD of each Gaussian atom. Specifically, the MWD TFR is defined as

$$\text{MWD}_x(t) = \sum_{i=0}^{L-1} |\beta_i|^2\, W_{g_{\gamma_i}}(t, f)$$

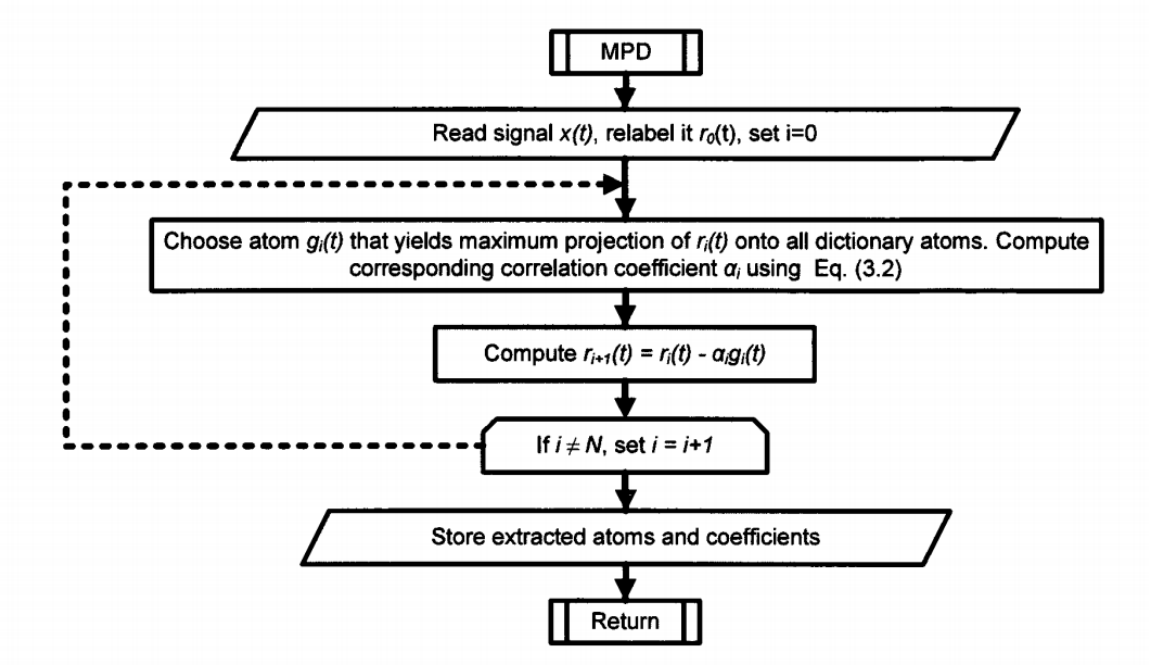

Figure 2.2: Block Diagram of the MPD Algorithm (Taken From [1])

where the WD of $g(t)$ is given by

$$W_g(t,f) = \int g\left(t+\frac{\tau}{2}\right)\, g^*\left(t-\frac{\tau}{2}\right)\, e^{-j2\pi\tau f}\, d\tau\,. \tag{2.11}$$

The WD preserves time shifts, frequency shifts and scale changes on the analysis signal $x(t)$. Specifically,

$$x_1(t) = x(t-\tau) \Rightarrow W_{x_1}(t,f) = W_x(t-\tau, f) \tag{2.12}$$

$$x_2(t) = x(t)e^{j2\pi\nu t} \Rightarrow W_{x_2}(t,f) = W_x(t, f-\nu) \tag{2.13}$$

$$x_3(t) = \sqrt{|a|}x(at) \Rightarrow W_{x_3}(t,f) = W_x(at, f/a) \tag{2.14}$$

τ is the time shift, ν is the frequency shift, a is the scale parameter. As a result, the MPD

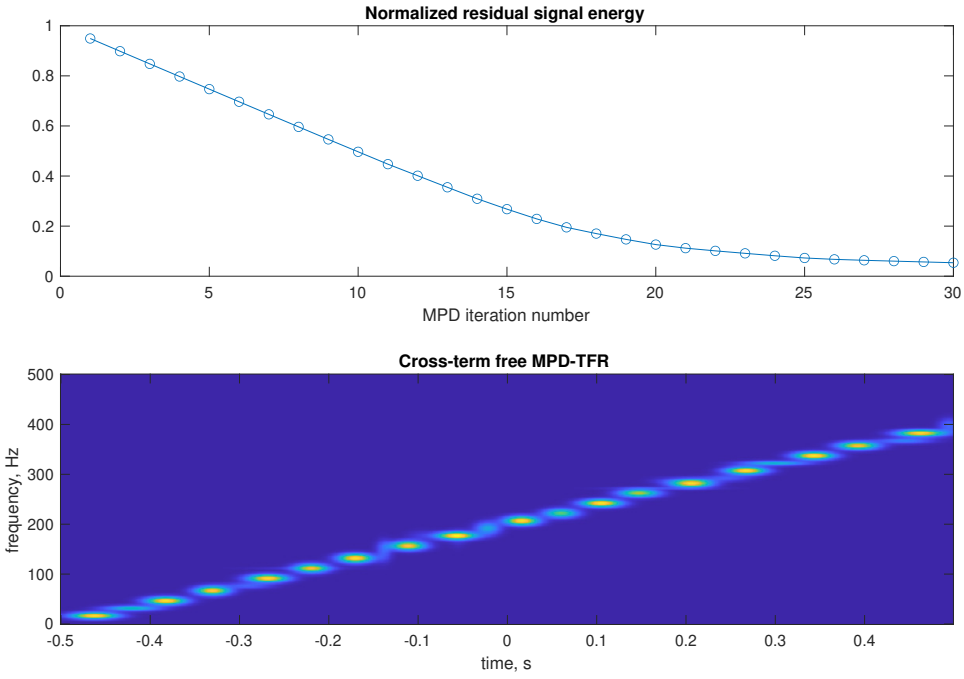

Figure 2.3: Example of the MPD of an LFM Signal.

can be simplified to

$$\text{MWD}_x(t) = \sum_{i=0}^{L-1} |\beta_i|^2 \, W_g\left(a_i(t-\tau_i), \frac{f-\nu_i}{a_i}\right)$$

An example of the MWD of an MPD decomposed LFM signal is is shown in Figure 2.3. The same LFM signal, but with additive white Gaussian noise, is also decomposed and shown in Figure 2.4. The residual signal energy after each iteration, together with the resulting MWD, are shown in Figures 2.4(a) and 2.4(b) for $L = 30$ and $L = 60$ MPD iterations. As it can be seen, after a certain number of iterations, most of the signal energy has been extracted. Thus, as the number of iterations increases, the residual signal energy decreases very slowly and more noise terms are included in the decomposition.

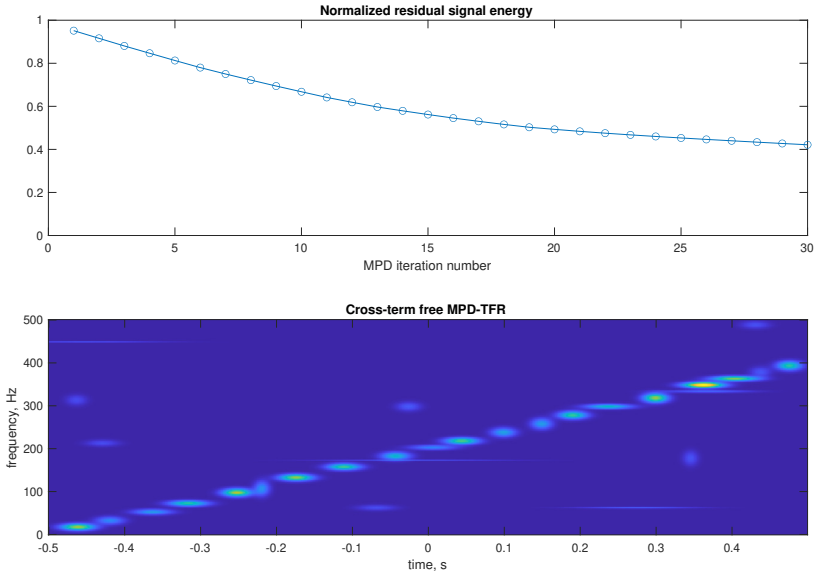

(a)

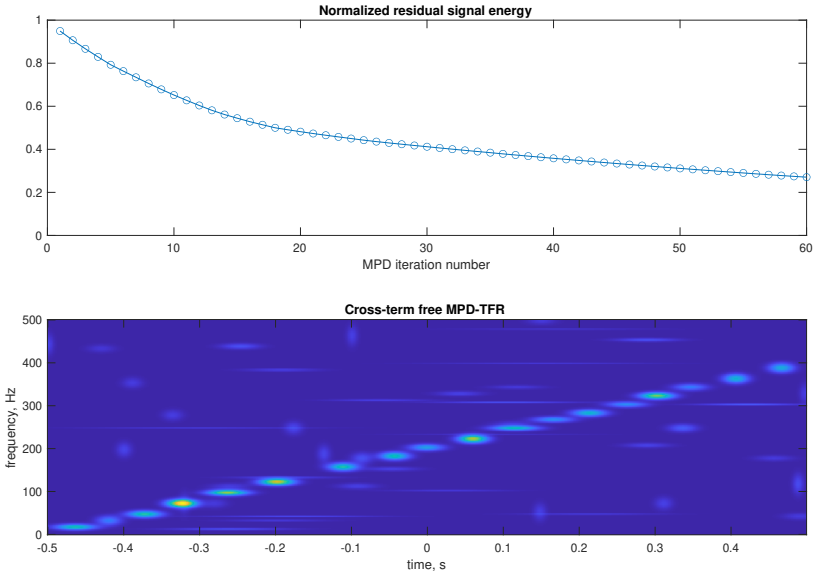

(b)

Figure 2.4: MMPD TFR of a Noisy LFM Signal, Using (a) 30 and (b) 60 MPD Iterations.

2.3 Gaussian Mixture Modeling

A Gaussian mixture model (GMM) is a probabilistic model that assumes that all measurements originated from a mixture of M Gaussian components. It is given by a weighted sum of M Gaussian probability density functions (PDFs) parameterized by their corresponding mean and covariances. Specifically, the PDF of an N-dimensional observation vector $\mathbf{z} = [z_1 \; z_2 \; \ldots \; z_N]^T$ can be expressed as a set of Gaussian mixtures

$$p\left(\mathbf{z} \mid \boldsymbol{\phi}\right) = \sum_{m=1}^{M} b_m \, \mathcal{N}\left(\mathbf{z}; \boldsymbol{\mu}_m, C_m\right) \tag{2.15}$$

Here, $\boldsymbol{\mu}_m$ is the mean vector, C_m is the covariance matrix, and b_m is the weight of the mth GMM mixture, $m = 1, \ldots, M$. Each component PDF is given by [49, 50, 51] where

$$p\left(\mathbf{z} \mid \boldsymbol{\phi}\right) = \mathcal{N}\left(\mathbf{z}; \boldsymbol{\mu}_m, C_m\right) = \frac{1}{\sqrt{(2\pi)^N \left|C_m\right|}} \exp\Big(-\frac{1}{2} \left(\mathbf{z} - \boldsymbol{\mu}_m\right)^T C_m^{-1} \left(\mathbf{z} - \boldsymbol{\mu}_m\right)$$

and the weights are such that

$$\sum_{m=1}^{M} b_m = 1$$

The GMM parameters can be optimally estimated to best match the characteristics of the observation $\mathbf{z}$. The most common of estimating the parameters is using maximum likelihood estimation, as discussed in Section 2.1. In particular, the mean and covariance of each Gaussian model is estimated using the expectation-maximization (EM) algorithm [44, 50, 52].

The GMM parameter vector in Equation (2.15) is $\boldsymbol{\phi} = [\boldsymbol{\Phi}_1 \; \ldots \; \boldsymbol{\Phi}_M]$, where $\boldsymbol{\Phi}_m = \{b_m, \boldsymbol{\mu}_m, C_m\}$. This vector can also be learned by putting prior PDFs on the parameters.

These PDFs include the Dirichlet distribution conjugate prior to model the weight b_m and the normal inverse Wishart distribution conjugate prior to model $\boldsymbol{\mu}_m, C_m$.

Chapter 3

NEW METHOD FOR TIME DELAY ESTIMATION

3.1 Problem Formulation

We consider the problem of tracking the position of an object using radar noisy measurements. The tracking scenario is complicated by the complex environment, where the radar shares its available spectrum with a wireless multiuser communications system. As the radar and communications system coexist, the radar receiver considers the communications signal as interference that is corrupting the estimation performance. As a result, the radar receiver must process the overall received signal taking into account not only the presence of noise but also the presence of interference

We assume that the radar transmits a linear frequency-modulated (LFM) signal

$$s(t;\alpha) = e^{j2\pi\alpha\, t^2}$$

with frequency modulation (FM) rate α Hz^2. The FM rate is assumed known at the radar receiver. After transmission, the LFM signal is reflected off the object and the received echo is observed at the receiver. The overall signal also includes multiple transmitted signals from a multiuser communications system. The users are assumed to employ a frequency modulation signaling scheme. Specifically, the signal of the lth communication user is

given by the sinusoid

$$y_l(t; f_l) = e^{j2\pi f_l t}, \quad l = 1, \ldots, L\,.$$

where each user is assumed to have a unique transmit frequency f_l Hz. After detection, the overall noisy baseband received signal is processed at the receiver to estimate the time delay of the transmitted LFM signal.

For processing, the real part of the received signal is given by

$$\begin{aligned} x(t) &= s(t-\tau;\alpha) + y_1(t; f_1) + \ldots + y_L(t; f_l) + w(t) \\ &= \cos\left(2\pi\alpha\,(t-\tau)^2\right) + \cos\left(2\pi f_1 t\right) + \ldots + \cos\left(2\pi f_L t\right) + w(t) \\ &= z(t;\alpha,\tau) + \sum_{l=1}^{L} y_l(t; f_l) + w(t) \end{aligned} \tag{3.1}$$

where $w(t)$ is assumed to be additive white Gaussian noise. The delayed LFM signal is given by $z(t;\alpha,\tau) = s(t-\tau;\alpha) = \cos\left(2\pi\alpha\,(t-\tau)^2\right)$, where τ seconds is the time delay. Note that the receiver does not have knowledge of the frequencies of the communications users. Also, the number of users L that are transmitting at any given time is unknown and varying with time.

The radar tracking goal is to estimate the range of the object by estimating the time delay using the received signal $x(t)$. Once we obtain the estimated time delay $\hat{\tau}$, the range r, in meters (m), is computed as

$$r = \frac{c\,\hat{\tau}}{2}$$

where $c = 3\times10^8$ m/s is the speed of electromagnetic waves in air. Note that, when an LFM

signal is shifted in time by τ, the transformation is equivalent to shifting the same LFM signal in frequency $-2\alpha\tau$ Hz and adding a constant phase change. The transformation is shown for the baseband signal as

$$\begin{aligned} s(t-\tau;\alpha) &= e^{j2\pi\alpha\,(t-\tau)^2} = e^{j2\pi\alpha\,(t^2-2t\tau+\tau^2)} \\ &= e^{j2\pi\alpha\,t^2}\, e^{j2\pi(2\tau\alpha)\,t}\, e^{j2\pi\alpha\,\tau^2} \\ &= s(t;\alpha)\, e^{j2\pi(2\tau\alpha)\,t}\, e^{j2\pi\alpha\,\tau^2}\,. \end{aligned} \tag{3.2}$$

The frequency shift is also demonstrated using the Fourier transform (FT) of the time-delayed LFM signal. Specifically, denoting the FT of $s(t)$ by $S(f)$ and using FT signal properties, it can be shown that

$$s(t-\tau) = s(t)\, e^{-j2\pi(2\tau\alpha)\,t}\, e^{j2\pi\alpha\,\tau^2} \overset{\text{FT}}{\longleftrightarrow} S(f+2\tau\alpha)\, e^{j2\pi\alpha\,\tau^2}\,. \tag{3.3}$$

For processing, we obtain discrete signal samples $x[n] = x(nT_s)$, $n = 0, \ldots, N-1$, where T_s is the sampling period. The transmitter uses the sample sampling period, so the sampled transmitted signal is $s[n] = s(nT_s)$, $n = 0, \ldots, M-1$, where $M < N$. Note that a larger number of samples is needed at the receiver to account for the time delay. The received signal samples are given by

$$\begin{aligned} x[n] &= s[n-\chi;\beta] + c[n;\kappa_1] + ... + c[n;\kappa_l] + w[n] \\ &= \cos\left(2\pi\beta\,(n-\chi)^2\right) + \cos\left(2\pi n\kappa_1\right) + \ldots + \cos\left(2\pi n\kappa_L\right) + w[n] \\ &= \cos\left(2\pi\beta\,(n-\chi)^2\right) + \sum_{l=1}^{L}\cos\left(2\pi n\kappa_l\right) + w[n] \end{aligned} \tag{3.4}$$

Here, $\chi = \lceil \tau / T_s \rceil$ is the discrete time delay of the LFM signal, $\kappa_l = f_1 l \, T_s$ is the lth discrete modulation frequency of the lth communications user, and $\beta = \alpha \, T_s^2$ is the (unitless) FM rate. The Gaussian noise samples $w[n]$ in Equation (3.4) are assumed independent and identically distributed with zero mean and variance σ^2. Note that the noise samples and communications signal samples are assumed to be present over all N received samples.

3.2 Proposed Time Delay Estimation Approach

At the radar receiver, we need to estimate the time shift χ of the LFM signal. This is similar to the maximum likelihood estimation problem we considered in Section 2.1.2 in Chapter 2, except that the signal samples now include an added interference term in addition to the noise term. As a result, the receiver would have to also estimate the variance of the noise as well as the intensity of the interference, which cannot be assumed known in a real tracking scenario. Note that the noise variance and the interference intensity are considered nuisance parameters [44]. This is because their estimated values have no other use other than in estimating the time delay. Also, finding the maximum likelihood estimates (MLEs) of the nuisance parameters will decrease the time delay estimation performance. As shown in [44], the overall estimation performance decreases as the number of unknown parameters increases [44].

We propose a new approach to increase the estimation performance of the LFM time delay parameter without the need to estimate nuisance parameters. The approach is based on two advanced signal processing methods, time frequency signal processing and ma-

chine learning. We first use the matching pursuit decomposition (MPD) time-frequency (TF) method to decompose the overall received signal. The extracted low-dimensionality feature vectors from the MPD are then used with a Gaussian mixture model (GMM) for clustering. The proposed approach provides two estimation methods, one based directly on the MPD and the other based on integrating the MPD with GMM clustering. We respectively refer to the two proposed estimation methods as modified matching pursuit decomposition based estimation method (MMPD-EM) and the modified Gaussian mixture model based estimation method (MGMM-EM).

3.2.1 Matching Pursuit Based Estimation Method

As discussed in Chapter 2, the Wigner distribution (WD) TF representation (TFR) provides the MLE of the unknown time shift of an LFM signals under known noise and interference conditions. The resulting MLE is given in Equation (3.7). We also showed in Chapter 2 that the TFR of an MPD decomposed signal provides a high localized representation in terms of TF shifted and scaled Gaussian signals $g_i(t)$. The TFR is the modified WD given by

$$\text{MWD}_x(t) = \sum_{i=0}^{\mathcal{L}-1} |b_i|^2 \, W_{g_{\gamma_i}}(t, f)$$

where $x(t)$ is the analysis signals and $\mathcal{L}$ is the number of MPD iterations.

The new MMPD-EM method combines these two results from Chapter 2. In particular,

we first decompose the radar received signal using the MPD iterative algorithm to obtain

$$x[n] = r_{\mathcal{L}}[n] + \sum_{i=0}^{\mathcal{L}-1} b_i \, g_{\gamma_i}[n]$$

Each of the L Gaussian atoms $g_{\gamma_i}[n]$ in the expansion has a unique four-dimensional vector given by

$$\gamma_i = [b_i \; \chi_i \; \kappa_i \; a_i]^T, \quad i = 0, \ldots, \mathcal{L} - 1 \tag{3.5}$$

where b_i is the MPD weight coefficient, $\chi_i = \tau_i / T_s$ is the time shift, $\kappa_i = \nu_i \, T_s$ is the frequency shift and a_i is the scale change.

We form the discrete MWD of the decomposed signal as

$$\text{MPD}_x[n, k] = \sum_{i=0}^{\mathcal{L}-1} |\beta_i|^2 \, \text{WD}_{g_{\gamma_i}}[n, k]$$

Using WD properties, as in Chapter 2, we use the MWD to estimate the unknown time delay χ as

$$\hat{\chi} = \arg \max_{\chi \in S_\chi} \frac{1}{M} \sum_{n=\chi}^{\chi+M-1} \text{MWD}_x[n, \lceil 2\,\beta\,(n - \chi) \rceil] \tag{3.6}$$

Here, $\mathcal{L}$ is the number of MPD iterations, and β and M are the FM rate the number of samples of the transmitted LFM signal. Also, the range of χ values is $S_\chi = \{1, N - M + 1\}$.

The proposed MMPD-EM methods thus estimates the time delay by maximizing the MWD of the MPD extracted Gaussians along lines in the TF plane; the slope of the line depends on the FM rate β. A simple example is shown in Figure 3.1. The parameters include 5 communication users and high SNR. The MPD iterates until its extracted energy is E is 70%. The actual time delay is $\tau = -0.25$ s and the range of user frequencies is $(500, 800)$ Hz. The red line is the estimation line of the LFM signal shown in the TF plane

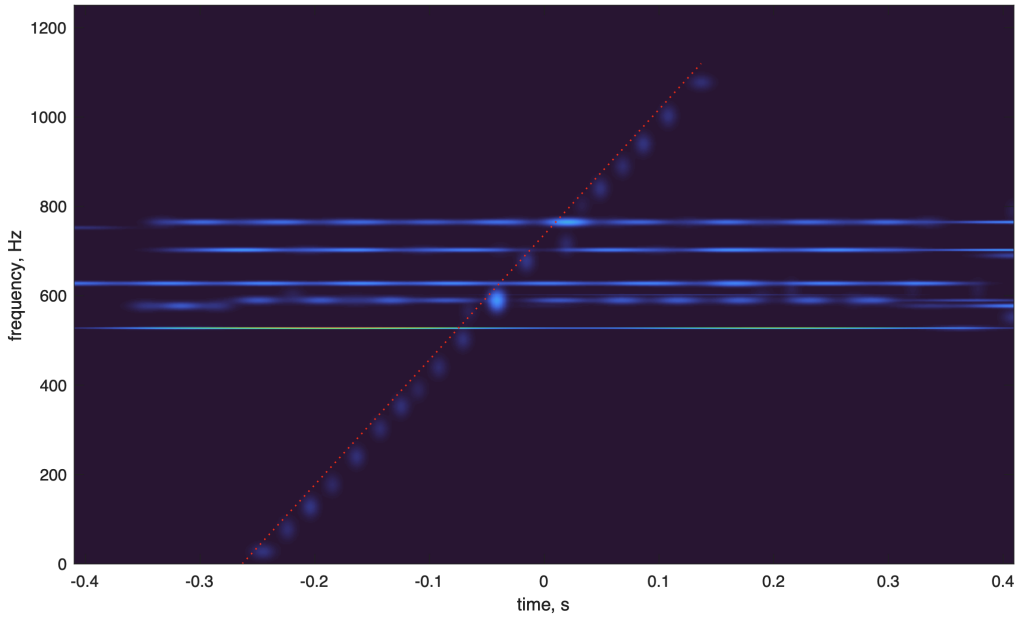

Figure 3.1: MMPD-EM Example

3.2.2 Gaussian Mixture Model Based Estimation Method

Using the result of the MPD from the previous section, we propose the MGMM-EM estimation method as follows. The MPD feature vectors in Equation (3.5) are used as input to a GMM algorithm for a fixed number of mixtures G. The resulting G clusters consist of a number of MPD Gaussian atoms, $\mathcal{R}_\ell$, $\ell = 1, \ldots, G$. Note that the number $\mathcal{R}_\ell$ varies, depending on the clustering outcome. The MGMM-EM estimator for the time delay is the minimum of all $\hat{\chi}_\ell$ values, where the time delay estimate of the ℓth cluster is given by

$$\hat{\chi}_\ell = \arg \max_{\chi \in S_\chi} \frac{1}{M} \sum_{n=\chi}^{\chi+M-1} \text{MWD}_{g_\ell}[n, \lceil 2\,\beta\,(n-\chi) \rceil\,]$$

Here, g_ℓ are all the Gaussian atoms in the ℓth cluster. This method is demonstrated in Figure 3.2 for the same parameters used in the MMPD-EM example.

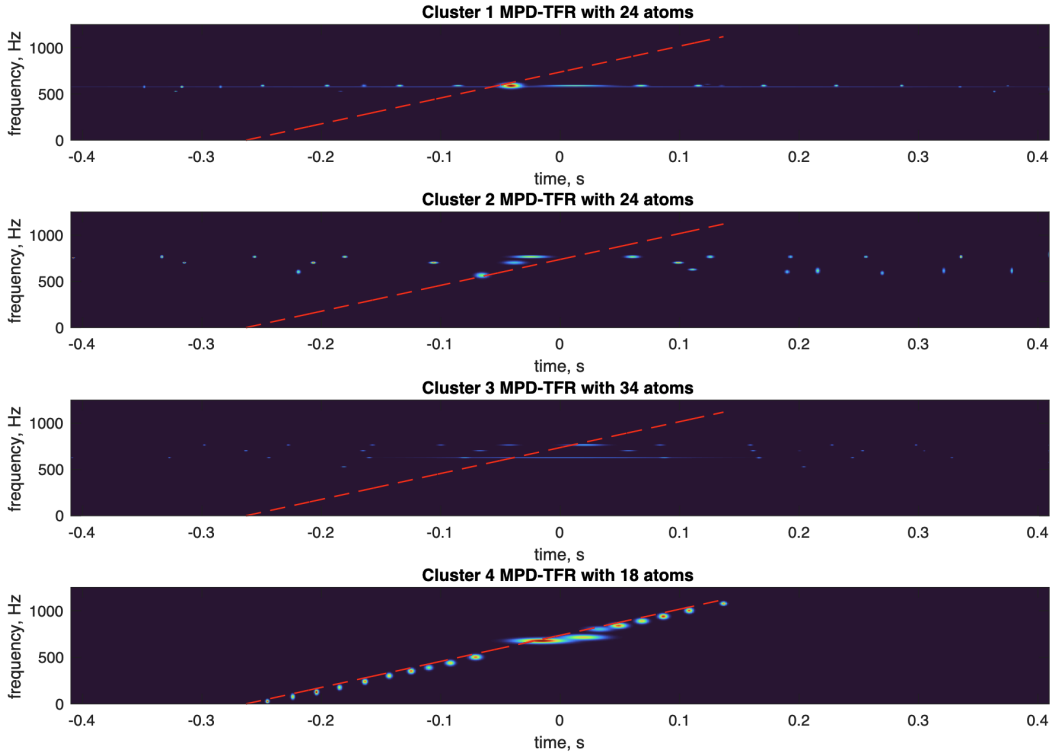

Figure 3.2: MGMM-EM Example

Chapter 4

SIMULATIONS AND DISCUSSION

4.1 Simulation Parameters

In this chapter, we simulate various scenarios of estimating the position of an object using radar sensor measurements. The simulations provide comparison of three estimation methods: the Wigner distribution based estimation method (WD-EM), the proposed modified matching pursuit decomposition(MPD) based estimation method (MMPD-EM) and the proposed modified matching pursuit decomposition with Gaussian mixture modeling based estimation method (MGMM-EM).

For all simulations, the goal is to estimate the time delay τ of the radar transmit signal that is observed at the radar receiver. The radar transmits a linear frequency-modulated (LFM) chirp $s(t) = \cos(2\pi\alpha t^2)$, $t \in (0, T_{\text{tr}})$. At the radar receiver, the overall measurement is given by $x(t) = s(t-\tau) + z_L(t) + w(t)$, $t \in (0, T_{\text{rec}})$. Unless otherwise stated, all simulations assume that the radar shares its available spectrum with a multi-user wireless communications system. The communications received signal is given by $z_L(t) = \sum_{\ell=1}^{L} z_\ell(t)$, where $z_\ell(t) = \cos(2\pi f_\ell t)$, f_ℓ is the unique modulation frequency of the ℓth user, $\ell = 1, \ldots, L$, and L is the total number of communication users. The user frequencies $\{f_1, \ldots, f_L\}$ uniformly selected within a given frequency band B_L. At the radar receiver, $z_L(t)$ is considered added interference that affects the time delay estimation per-

formance of the radar. The received signal is also corrupted with zero-mean white Gaussian noise $w(t)$ with known variance σ^2. We vary the noise variance using a desired signal-to-noise ratio (SNR), which we compute as SNR $= 10\log_{10}(E_s/\sigma^2)$ in dB, where E_s is the transmit signal energy. Both the MMPD-EM and MGMM-EM methods use the iterative MPD algorithm with the stopping criteria: a fixed percentage of the decomposed signal energy E. Unless otherwise stated, the same parameters will be used for both methods in each scenario. The MGMM-EM is assumed to use G GMM clusters.

The fixed signal and algorithm parameters used in our varying simulation examples are listed in Table 4.1. The table includes the sampling frequency f_s in Hz, signal durations T_{tr} in seconds (s), number of GMM clusters G, MPD stopping criteria (energy percentage in MPD) E, frequency modulation (FM) rate α in Hz^2, maximum LFM frequency $f_{\max} = 2\alpha T_{\text{tr}}$ in Hz (should be less than $f_s/4$), and the actual (true) time delay τ in s, number of communication users L, user frequency range B_L in Hz and signal to noise ratio SNR in dB. Unless otherwise stated, the scenario in the table all have 2k Monte Carlo(MC) runs. Note that Monte Carlo simulations are used to account for the randomness of both the noise and the uniform selection of communication user frequencies.

Note that the time delay estimation performance is compared using the estimation root mean-squared error (RMSE) in seconds. It is computed as

$$\text{RMSE} = \left(\frac{1}{\text{MC}} \sum_{m=1}^{\text{MC}} (\tau - \hat{\tau})^2 \right)^{1/2} \tag{4.1}$$

where $\hat{\tau}$ is the estimated time delay. For the MGMM-EM, $\hat{\tau}$ is the minimum of G estimated values at each of MC iteration.

Signal Parameters								
f_s,Hz	T_{tr},s	G	E	α,Hz^2	τ,s	L	B_L,Hz	SNR,dB
Scenario 1: Varying Energy Stopping Criteria								
2.5	0.4	5	varies	600	-0.25	10	(100, 400)	15,25
Scenario 2: Varying Clusters Number								
2.5	0.4	varies	70%	600	-0.25	10	(100, 400)	15,25
Scenario 3: Low SNR with No Spectrum Sharing								
1.2	0.18	6	90%	700	-0.18	5	(500, 800)	varies
Scenario 4: Low SNR with Spectrum Sharing								
1.2	0.18	6	70%	700	-0.18	5	(100, 200)	varies
Scenario 5: Varying SNR with Small Spectrum Sharing								
1.2	0.18	6	90%	700	-0.18	5	(200, 400)	varies
Scenario 6: Varying SNR with Spectrum Sharing								
1.2	0.18	6	30%,70%,90%	700	-0.18	5	(100, 200)	varies
Scenario 7: Varying SNR with Different Parameters								
2.5	0.4	5	30%, 70%	600	-0.25	10	(100, 400)	varies

Table 4.1: Signal Parameters in Different Scenarios

4.2 Simulation Scenarios

4.2.1 Varying MPD Stopping Criteria in Scenario 1

The simulations in this scenario compare the time delay estimation RMSE results for different MPD stopping criteria with both 15 and 25 dB SNR, and with 2 k MC runs. The signal parameters are provided in Table 4.1. In Figure 4.1, note that there are 10 communication users, 5 GMM clusters, the maximum LFM frequency is 560 Hz and the range of user frequencies is $(100, 400)$ Hz.

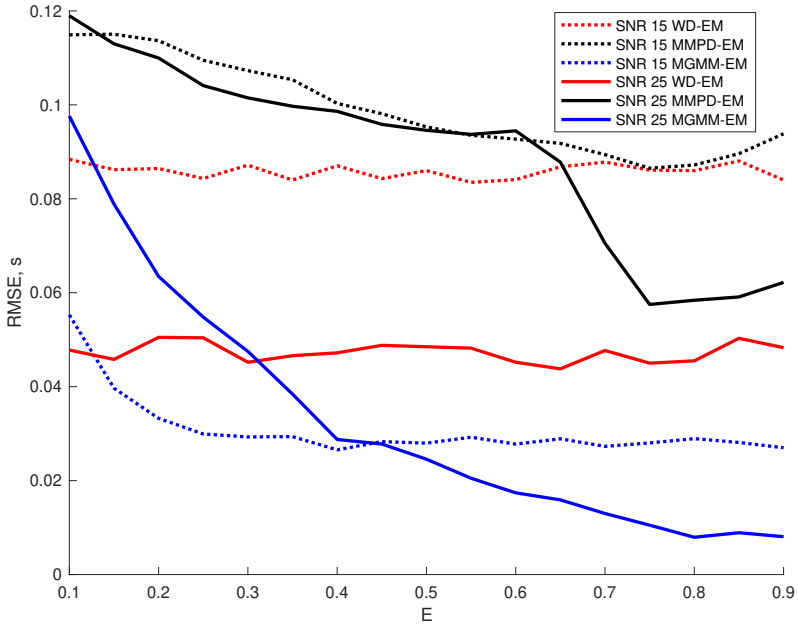

Figure 4.1: RMSE vs Varying MPD Energy Stopping Criteria in Scenario 1

From the Figure, the MGMM-EM outperforms both of the other methods for the chosen SNR values if the MPD stopping criteria is larger than 30%. Note that the performance

of WD-EM decreases (RMSE is larger) with more noise (SNR is smaller). In order to compare the detailed performance of MGMM-EM and MMPD-EM, we plot both methods separately.

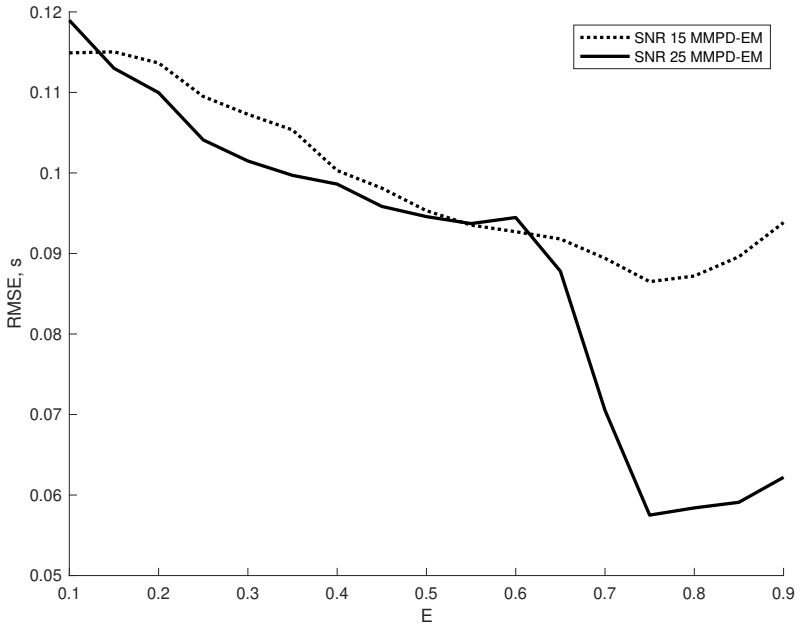

Figure 4.2: MMPD-EM RMSE vs Varying MPD Energy Stopping Criteria

In Figure 4.2, the performance of MMPD-EM increases when the MPD stopping energy criteria increase from 10% to 75%, after that the performance decreases even if we keep increasing the energy threshold. The reason for this phenomenon is that when the MPD has too many energy in the TFR, the noise will takes a large place of the decomposed signal, so the time-delay finding process will be more difficult. That is why we should choose the MPD Energy Stopping Criteria around 75% in order to have the best performance for MMPD-EM.

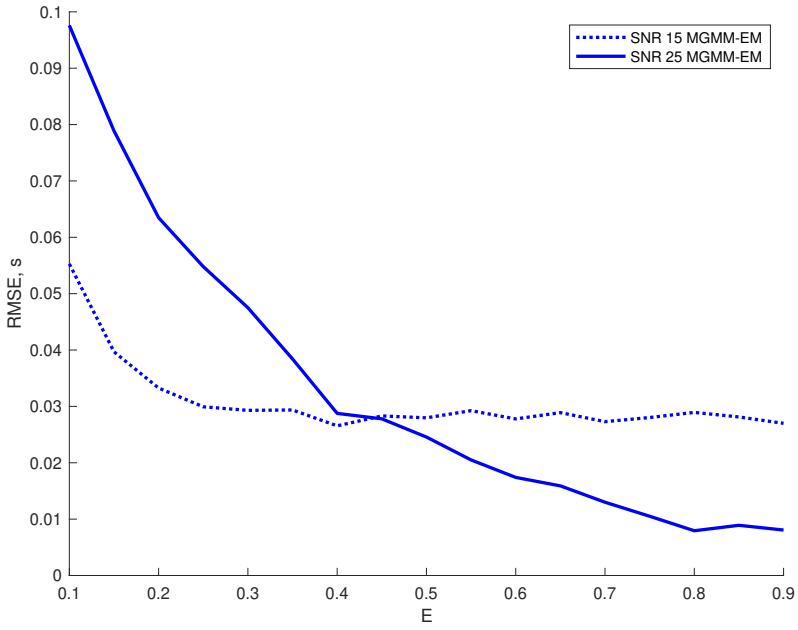

Figure 4.3: MGMM-EM RMSE vs Varying MPD Energy Stopping Criteria

In Figure 4.3, if we consider the signal with very little noise, the performance of MGMM-EM will increase when the MPD stopping energy criteria keep increasing. However, we should consider the computational expenses of the MPD, since the more energy we want, the more iteration times are needed. Besides, if we take noise into consideration (SNR 15), the performance of MGMM-EM stayed almost the same after 25% energy threshold. Therefore, in MGMM-EM, we can keep the energy threshold considerably small to avoid huge computational expenses.

In addition, in Table 4.2, we compare under different SNR, the iteration times related to different energy threshold. It shows the more energy threshold we choose, the more iteration times we need. Besides, the more noise we have, the more iteration times we

need. This results further demonstrate the huge computational expenses when we want more energy in the MPD-TFR. That is why the MGMM-EM is a better way, sicne it does not need large energy threshold than MMPD-EM.

Different	Mean Iteration Times: Varying E								
Noise Level	0.1	0.2	0.3	0.4	0.5	0.6	0.7	0.8	0.9
SNR 25	3	6	11	17	26	39	58	106	221
SNR 15	8	20	39	63	93	132	181	250	364

Table 4.2: Mean Iteration Times in Scenario 1

4.2.2 Varying Number of GMM Clusters in Scenario 2

The simulations in this scenario compare the time delay estimation RMSE results for different number of GMM clusters with both 15 and 25 dB SNR, and with 2 k MC runs. The signal parameters are provided in Table 4.1. In Figure 4.4, note that there are 10 communication users, the MPD energy stopping criteria is 70%, the maximum LFM frequency is 560 Hz and the range of user frequencies is $(100, 400)$ Hz.

From the Figure, the MGMM-EM also outperforms both of the other methods for the chosen SNR values. Note that in this simulation the performance of WD-EM is better than MMPD-EM because we do not give the MMPD-EM enough iteration times (energy threshold). In order to compare the detailed performance of MGMM-EM with the cluster numbers, we plot this method separately.

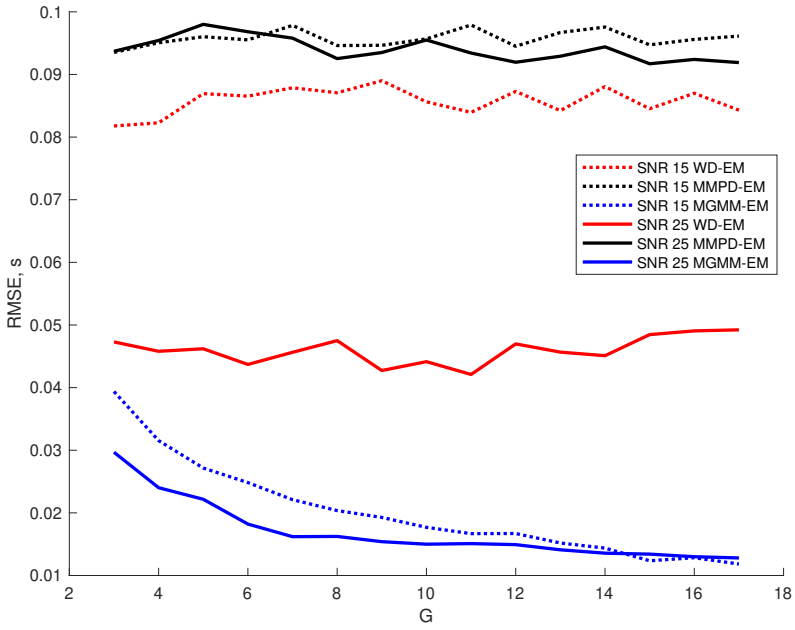

Figure 4.4: RMSE vs Varying Number of Clusters in Scenario 2

In Figure 4.5, no matter in what noise level , the performance of MGMM-EM will increase when the number of GMM clusters keep increasing. For example, the error is only 8% related to the time delay 0.25 with 25dB SNR and 5 clusters for GMM, which is relatively small compared with other methods. Therefore, we should also consider the computational expenses here if we want to achieve a cost-effective performance.

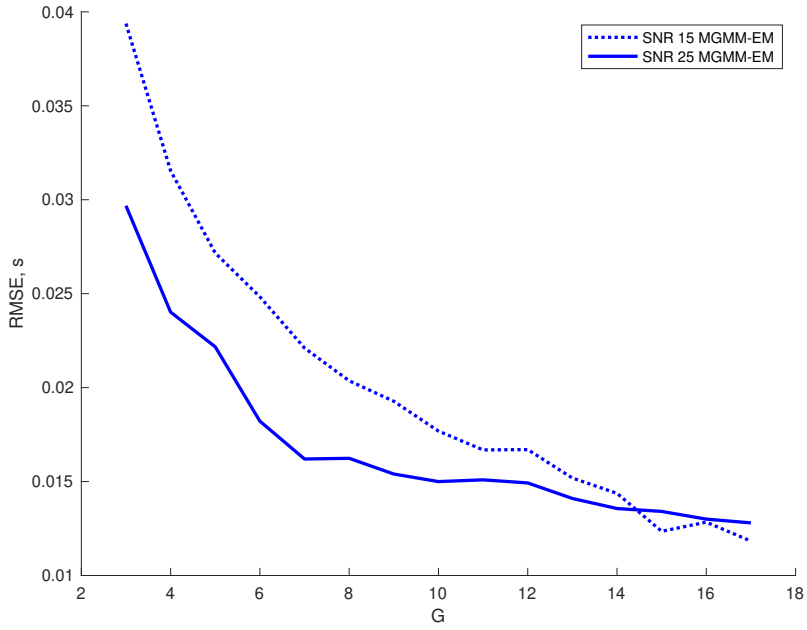

Figure 4.5: MGMM-EM RMSE vs Number of Clusters

4.2.3 Low SNR Conditions Without Spectrum Sharing in Scenario 3

The simulations in this scenario compare the time delay estimation RMSE results for low SNR values. The signal parameters are provided in Table 4.1 and the results are summarized in Table 4.3.

Note that the radar and communication systems do not share spectrum; the maximum LFM frequency is 252 Hz and the range of user frequencies is $(500, 800)$ Hz, the number of communication users is 5, MPD stopping criteria is 90%, GMM cluster number is 6, and 5 k MC runs. From the table, the MGMM-EM outperforms both of the other methods for all low SNR values. It shows that WD-EM and MMPD-EM perform about the same when the communication signaling and the LFM radar do not overlap in frequency.

Estimation Method	RMSE: Varying SNR, $B_L = (500, 800)$ Hz				
	-20 dB	-16 dB	-11 dB	-7 dB	-2 dB
WD-EM	0.1072	0.1090	0.1096	0.1115	0.1086
MMPD-EM	0.1128	0.1169	0.1188	0.1193	0.1155
MGMM-EM	0.0234	0.0245	0.0237	0.0241	0.0227

Table 4.3: RMSE Comparison in Scenario 4 with Low SNR and No Spectrum Sharing

4.2.4 Low SNR Conditions with Spectrum Sharing in Scenario 4

This simulation is similar to the one in Section 4.2.3 in that most of its parameters are the same as those in Scenario 3. However, it uses two higher SNR values and also the two systems now share spectrum. In particular, the range of user frequencies $(100, 200)$ Hz is now decreased while the maximum LFM frequency remains at 252 Hz. The time delay estimation RMSE results are summarized in Table 4.4 and shown to be similar to those in Section 4.2.3. Note that since there are only $E = 70\%$ energy threshold (instead of 90%), the MMPD-EM performs better than the WD-EM for higher SNR values.

Estimation Method	RMSE: Varying SNR, $B_L = (100, 200)$ Hz				
	-30 dB	-20 dB	-10 dB	0 dB	10 dB
WD-EM	0.1098	0.1069	0.1094	0.1082	0.0983
MMPD-EM	0.1200	0.1171	0.1153	0.1130	0.0963
MGMM-EM	0.0245	0.0225	0.0238	0.0228	0.0183

Table 4.4: RMSE Comparison in Scenario 4 with Low SNR and Spectrum Sharing

4.2.5 Varying SNR with Small Spectrum Sharing in Scenario 5

This simulation is similar to the one in Section 4.2.4 in that most of its parameters are the same as those in Scenario 4. However, the range of user frequencies is changed to $(200, 400)$ Hz, which means the overlap is not as many as the situation in Scenario 4.

The time delay estimation RMSE results are shown in Figure 4.6. It shows that all 3 methods work well for high SNR, but the MGMM-EM outperform the other two methods when SNR is smaller than 25dB.

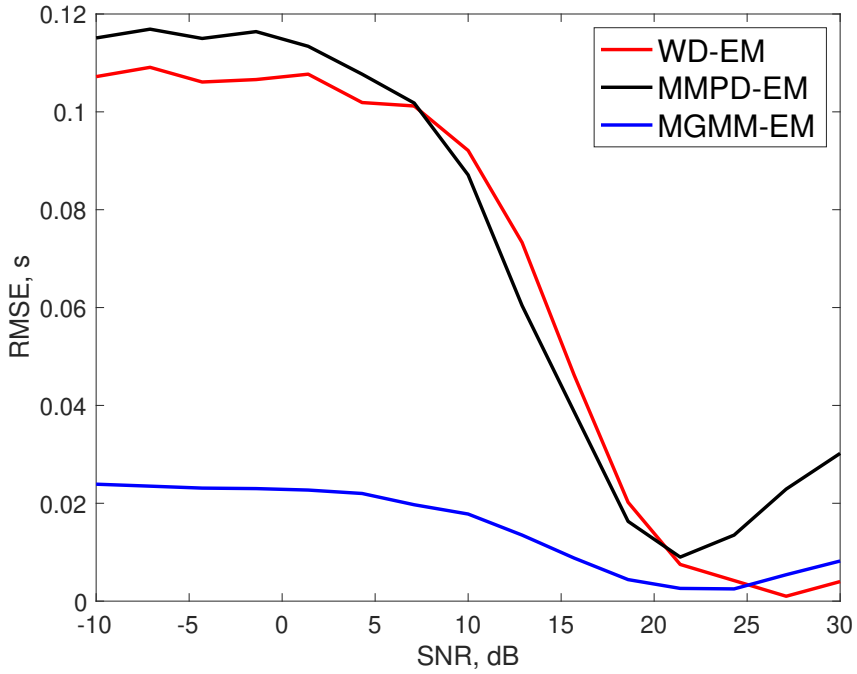

Figure 4.6: RMSE vs Varying SNR in Scenario 5

4.2.6 Varying SNR with Spectrum Sharing in Scenario 6

This simulation uses the signal parameters from Scenario 4 in Table 4.1. The number of communication users is $L = 5$ with frequency range $B_L = (100, 200)$. As the LFM maximum frequency is 252 Hz, all 5 communication users share spectrum with the radar. The algorithm parameters are $G = 6$ GMM clusters, and 2k MC runs. There are 3 different MPD energy stopping criteria ($E = 0.3$, $E = 0.7$,and $E = 0.9$), so we can verify the discussion in scenario 1 about the performance of MMPD-EM and MGMM-EM with energy threshold. The RMSE performance comparison is demonstrated in Figure 4.7.

From the Figure, the MGMM-EM outperforms both of the other methods for all SNR

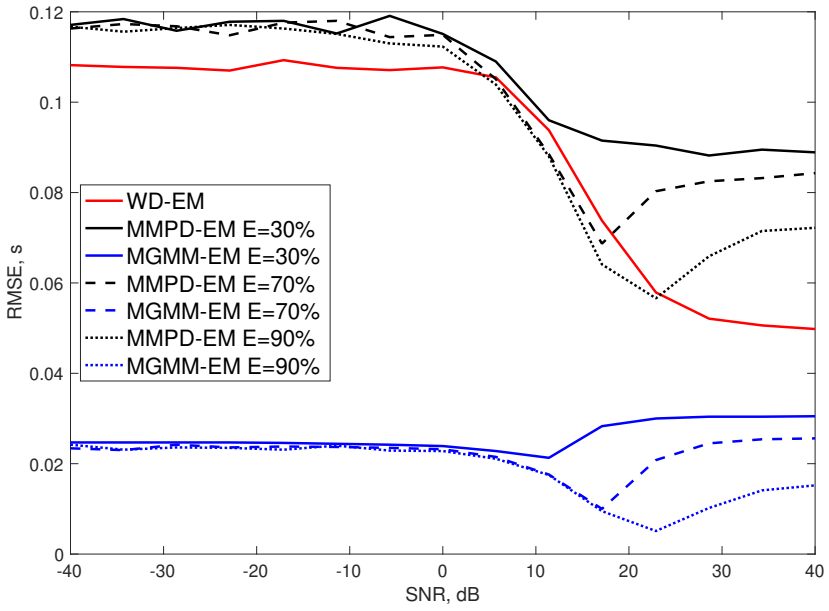

Figure 4.7: RMSE vs Varying SNR in Scenario 6

values. However we noticed that there are points between SNR 10dB and 30dB where before them the performances for both MGMM-EM and MMPD-EM increase when the noise is smaller, after them the performances decrease when the noise keeps getting smaller. Besides, the performance of MMPD-EM with 30% energy threshold will not decrease after the point when the noise keeps getting smaller. In order to see if that is a special case for the signal we choose, we change the parameters and do Monte Carlo simulations again in scenario 6.

4.2.7 Varying SNR with Different Parameters in Scenario 7

This simulation uses the signal parameters from Scenario 1 and 2 in Table 4.1. Note that, when compared to the parameters in Scenario 6, both the transmitted and received

signals are now longer. The number of communication users is $L = 10$ with frequency range $B_L = (100, 400)$. As the LFM maximum frequency is 560 Hz, all 10 communication users share spectrum with the radar. The algorithm parameters are $G = 5$ GMM clusters, and 2k MC runs. There are only 2 different MPD energy stopping criteria ($E = 0.3$, $E = 0.7$), since in scenario 5 we find out that $E = 0.7$ and $E = 0.9$ have the same changing pattern. The RMSE performance comparison is demonstrated in Figure 4.8.

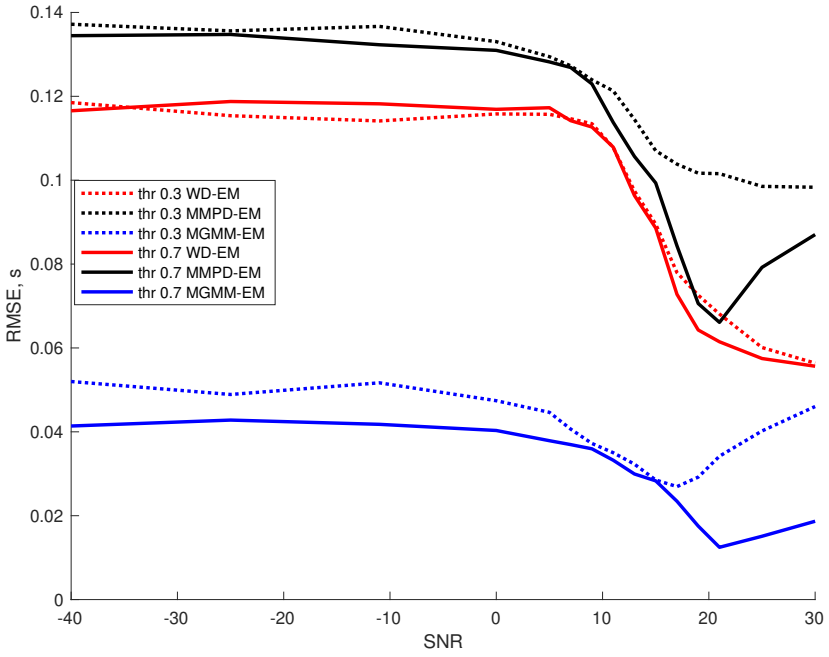

Figure 4.8: RMSE vs Varying SNR in Scenario 7

From the Figure, the MGMM-EM outperforms both of the other methods for all SNR values. Besides, we can see that the performances of WD-EM, MGMM-EM, and MMPD-EM in scenario 7 have the same changing patterns as in scenario 5, which disproves the randomness of the performance decreases after the points when the noise keeps getting

smaller. In order to analyse the detail, we plot the RMSE of MGMM-EM and MMPD-EM separately in Figure 4.9.

Note that with energy threshold equal to 30%, the RMSE of MMPD-EM will not increase after SNR 21dB. However, the RMSE of MMPD-EM will increase after 21 dB when the energy threshold is equal to 70%. The same situation appears in the MGMM-EM only with different SNR values. When SNR is around 30dB, there is almost no noise in the signal, which means basically only 70% of the LFM signal is in the MPD-TFR. The insufficient of the decomposed signal may cause the performance to decrease.

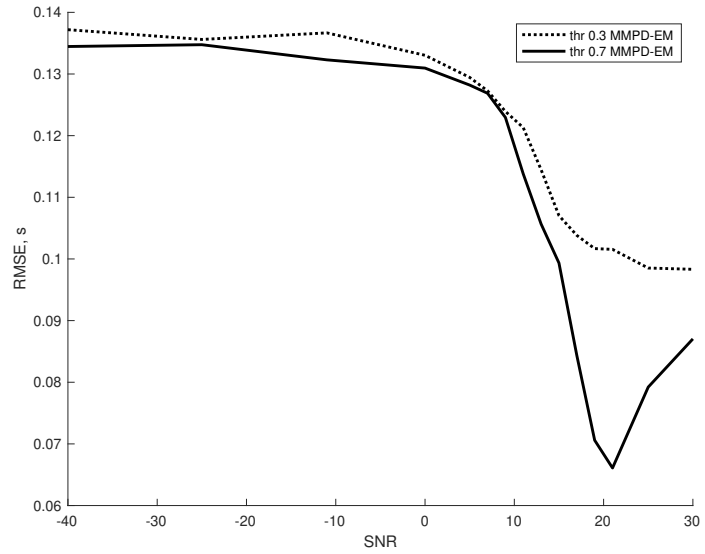

(a) MMPD-EM

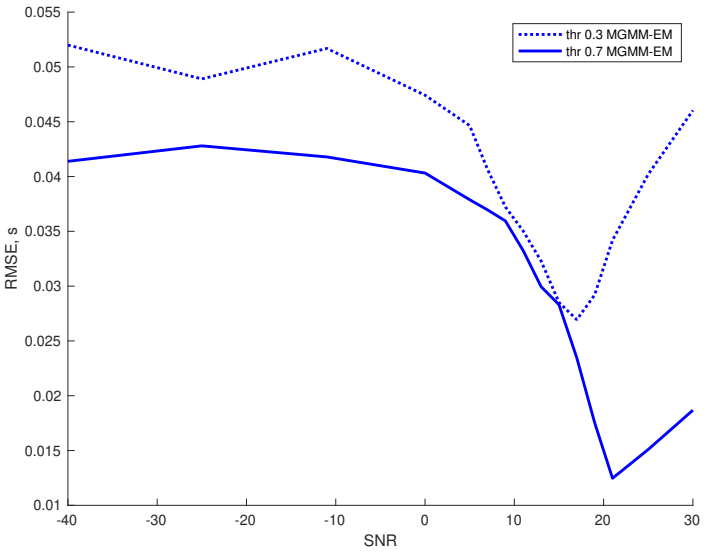

(b) MGMM-EM

Figure 4.9: MMPD-EM and MGMM-EM RMSE vs Varying SNR in Scenario 7

Chapter 5

CONCLUSIONS AND FUTURE RESEARCH DIRECTIONS

5.1 Conclusion

This thesis addressed the radar problem of estimating the position of an object under noisy conditions and with the radar sharing its spectrum with a multiuser communications system. In order to address to spectrum coexistence problem, we proposed a new approach to increase the object parameter estimation performance by integrating two advanced signal processing research areas, time-frequency signal processing and machine learning. The proposed approach provides two different methods for estimating the time delay of the linear frequency modulation (LFM) signal that is transmitted by the radar. The time delay estimate is then transformed to estimate the object position.

The first estimation method uses the matching pursuit decomposition (MPD) time-frequency (TF) algorithm to decompose the overall radar received signal. Using the MPD, a time-frequency representation (TFR) is obtained as a weighted linear combination of the Wigner distribution (WD) of each of the MPD extracted signal components. The WD is a well-known TFR that is highly localized for some signals, such as LFM and Gaussian signals. In particular, the WD of an LFM signal is a line in the TF plane whose slope depends on the frequency-modulation (FM) rate of the LFM signal. As we showed in Chapter 2, the maximum likelihood estimate (MLE) of the time shift of a noisy LFM signal, assum-

ing known conditions, is the time shift value that maximizes the sum of the WD of the received signal along lines in the TF plain. As the MPD decomposes the signal into TF shifted and scaled Gaussian signals, we use the WD of the MPD extracted signal components to estimate the time delay. The proposed modified MPD estimation method is based on maximizing the sum of the MPD-based TFR along lines in the TF plane.

The second estimation method is based on the MPD of the received signal. In particular, we use the MPD low-dimensional feature vectors, that consist of TF shift, scale change and coefficient parameters, as input to a Gaussian mixture model (GMM) for clustering. We then apply the TF maximization along lines method directly to the MPD-based TFR of the clustered Gaussian signal components.

Our simulations demonstrated the performance of the two proposed estimators and compared it to that of the WD-based estimator. We investigated multiple scenarios by varying critical parameters that can affect estimation performance. These parameters include the signal-to-noise ratio (SNR), the number of communications users interfering with the radar signal, the spectrum shared overlap between the two systems, stopping criteria of the iterative MPD algorithm and number of GMM clusters. As indicated by our simulations, GMM-based estimation method resulted in the highest performance, even under low SNR conditions and high interference. As expected, the three methods approach the same performance at very high SNR and low spectrum overlap.

5.2 Future Research Work

The proposed estimation methods can be modified to further improve their estimation performance. For example, the selection of the various parameters, such as the number of GMM clusters and the number of MPD iterations, can be optimized to achieve higher performance under specific optimization constraints. We also plan to investigate the computational complexity of the three methods and possible trade offs between computational cost and performance accuracy. Overall, the integration of signal processing with machine learning methods is very promising for use in other applications. One such application, following the demand of continued technological advances, is the coexistence of multiple different wireless modalities operating at much higher bandwidths.

REFERENCES

[1] D. Chakraborty, *Time-frequency based adaptive learning for structural health management*. PhD thesis, Arizona State University, 2010.

[2] S. Berger, "Spectrum congestion - is it a technical problem?," in *United States National Committee of URSI National Radio Science Meeting*, p. 1, 2014.

[3] D. Jokanovic and M. Josipovic, "RF spectrum congestion: Resolving an interference case," in *IEEE International inproceedings on Microwaves, Communications, Antennas and Electronics Systems*, pp. 1–4, 2011.

[4] R. H. Tehrani, S. Vahid, D. Triantafyllopoulou, H. Lee, and K. Moessner, "Licensed spectrum sharing schemes for mobile operators: A survey and outlook," *IEEE Communications Surveys Tutorials*, vol. 18, no. 4, pp. 2591–2623, 2016.

[5] A. Nehorai, M. Akcakaya, and S. Sen, "Special issue: Radar and information theory," *Entropy*, 2017.

[6] C. Masouros, R. W. Heath, J. A. Zhang, Z. Feng, L. Zheng, and A. P. Petropulu, "Editorial: Introduction to the issue on joint communication and radar sensing for emerging applications," *IEEE Journal of Selected Topics in Signal Processing*, vol. 15, no. 6, pp. 1290–1294, 2021.

[7] "Intenational Telecommunication Union." `https://www.itu.int/pub/r-rec/en`, February 2022. [Online; accessed 28-April-2022].

[8] National Academies of Sciences, Engineering, and Medicine, *Spectrum access: Allocation Policies and the Assignment Process*, ch. 7, pp. 147–160. The National Academies Press, 2015.

[9] E. Saltikoff, J. Y. Cho, P. Tristant, A. Huuskonen, L. Allmon, R. Cook, E. Becker, and P. Joe, "The threat to weather radars by wireless technology," *Bulletin of the American Meteorological Society*, vol. 97, pp. 1159–1167, 2016.

[10] S.-S. Raymond, A. Abubakari, H.-S. Jo, H.-J. Hong, and H. K. Son, "Compatibility between LTE and airport surveillance radar in 2700-2900 MHz radar bands," in *International inproceedings on Information and Communication Technology Convergence*, pp. 1037–1042, 2015.

[11] M. Spencer and F. Ulaby, "Spectrum issues faced by active remote sensing: Radio frequency interference and operational restrictions technical committee," *IEEE Geoscience and Remote Sensing Magazine*, vol. 4, pp. 40–45, 2016.

[12] J. R. Guerci, "Cognitive radar: A knowledge-aided fully adaptive approach," in *IEEE Radar inproceedings*, pp. 1365–1370, 2010.

[13] D. Garmatyuk, J. Schuerger, and K. Kauffman, "Multifunctional software-defined radar sensor and data communication system," *IEEE Sensors Journal*, vol. 11, no. 1, pp. 99–106, 2011.

[14] S. S. Bhat, R. M. Narayanan, and M. Rangaswamy, "Bandwidth sharing and scheduling for multimodal radar with communications and tracking," in *IEEE Sensor Array and Multichannel Signal Processing Workshop*, pp. 233–236, 2012.

[15] D. Bliss, "Cooperative radar and communications signaling: The estimation and information theory odd couple," in *IEEE Radar inproceedings*, pp. 50–55, 2014.

[16] J. Guerci and R. M. Guerci, "RAST: Radar as a subscriber technology for wireless spectrum cohabitation," in *IEEE Radar inproceedings*, 2014.

[17] M. R. Bell, N. Devroye, D. Erricolo, T. Koduri, S. Rao, and D. Tuninetti, "Results on spectrum sharing between a radar and a communications system," in *International Conference on Electromagnetics in Advanced Applications*, pp. 826–829, 2014.

[18] J. Guerci, R. Guerci, A. Lackpour, and D. Moskowitz, "Joint design and operation of shared spectrum access for radar and communications," in *IEEE Radar inproceedings*, pp. 761–766, 2015.

[19] A. Hassanien, M. G. Amin, Y. D. Zhang, and F. Ahmad, "Signaling strategies for dual-function radar communications: An overview," *IEEE Aerospace and Electronic Systems Magazine*, vol. 31, no. 10, pp. 36–45, 2016.

[20] S. Bhattarai, J.-M. J. Park, B. Gao, K. Bian, and W. Lehr, "An overview of dynamic spectrum sharing: Ongoing initiatives, challenges, and a roadmap for future research," *IEEE Transactions on Cognitive Communications and Networking*, vol. 2, pp. 110–128, 2016.

[21] M. Labib, V. Marojevic, A. F. Martone, J. H. Reed, and A. I. Zaghloui, "Coexistence between communications and radar systems: A survey," *URSI Radio Science Bulletin*, vol. 2017, no. 362, pp. 74–82, 2017.

[22] B. Paul, A. R. Chiriyath, and D. W. Bliss, "Survey of RF communications and sensing convergence research," *IEEE Access*, vol. 5, pp. 252–270, 2017.

[23] F. Liu, C. Masouros, A. P. Petropulu, H. Griffiths, and L. Hanzo, "Joint radar and communication design: Applications, state-of-the-art, and the road ahead," *IEEE Transactions on Communications*, vol. 68, pp. 3834–3862, 2020.

[24] A. Aubry, A. De Maio, Y. Huang, M. Piezzo, and A. Farina, "A new radar waveform design algorithm with improved feasibility for spectral coexistence," *IEEE Transactions on Aerospace and Electronic Systems*, vol. 51, no. 2, pp. 1029–1038, 2015.

[25] M. Bica, K.-W. Huang, U. Mitra, and V. Koivunen, "Opportunistic radar waveform design in joint radar and cellular communication systems," in *IEEE Global Communications*, pp. 1–7, 2015.

[26] J. G. Metcalf, C. Sahin, S. D. Blunt, and M. Rangaswamy, "Analysis of symbol-design strategies for intrapulse radar-embedded communications," *IEEE Transactions on Aerospace and Electronic Systems*, vol. 51, no. 4, pp. 2914–2931, 2015.

[27] B. Li, A. P. Petropulu, and W. Trappe, "Optimum co-design for spectrum sharing between matrix completion based mimo radars and a mimo communication system," *IEEE Transactions on Signal Processing*, vol. 64, no. 17, pp. 4562–4575, 2016.

[28] A. Hassanien, M. G. Amin, Y. D. Zhang, and F. Ahmad, "Dual-function radar-communications: Information embedding using sidelobe control and waveform diversity," *IEEE Transactions on Signal Processing*, vol. 64, no. 8, pp. 2168–2181, 2016.

[29] J. S. Kota, *Transmit waveform design for coexisting radar and communications systems*. PhD thesis, Arizona State University, 2016.

[30] V. S. Gattani, J. S. Kota, and A. Papandreou-Suppappola, "Time-frequency separation of matched-waveform signatures of coexisting multimodal systems," in *Asilomar inproceedings on Signals, Systems, and Computers*, pp. 2086–2090, 2018.

[31] J. S. Kota and A. Papandreou-Suppappola, "Joint design of transmit waveforms for object tracking in coexisting multimodal sensing systems," *Sensors, Special Issue Multiple Object Tracking: Making Sense of the Sensors*, vol. 19, 2019.

[32] S. Doly, A. R. Chiriyath, H. Mittelmann, D. Bliss, and S. Ragi, "Waveform codesign for radar-communications spectral coexistence via dynamic programming," *IEEE Transactions on Aerospace and Electronic Systems*, pp. 1–1, 2022.

[33] N. Nartasilpa, A. Salim, D. Tuninetti, and N. Devroye, "Communications system performance and design in the presence of radar interference," *IEEE Transactions on Communications*, vol. 66, pp. 4170–4185, 2018.

[34] F. Alberge, "Deep learning constellation design for the AWGN channel with additive radar interference," *IEEE Transactions on Communications*, vol. 67, pp. 1413–1423, 2019.

[35] J. Park, E. Lee, S.-H. Park, S.-S. Raymond, S. Pyo, and H.-S. Jo, "Modeling and analysis on radio interference of OFDM waveforms for coexistence study," *IEEE Access*, vol. 7, pp. 35132–35147, 2019.

[36] J. Johnston, Y. Li, M. Lops, and X. Wang, "ADMM-net for communication interference removal in stepped-frequency radar," *IEEE Transactions on Signal Processing*, vol. 69, pp. 2818–2832, 2021.

[37] J. Qian, L. Venturino, M. Lops, and X. Wang, "Radar and communication spectral coexistence in range-dependent interference," *IEEE Transactions on Signal Processing*, vol. 69, pp. 5891–5906, 2021.

[38] L. Cohen, *Time-Frequency Analysis*. Prentice-Hall, 1995.

[39] P. Flandrin, *Time-Frequency/Time-Scale Analysis*. Academic Press, 1999.

[40] A. Papandreou-Suppappola, ed., *Applications in Time-Frequency Signal Processing*. CRC Press, 2002.

[41] S. G. Mallat and Z. Zhang, "Matching pursuits with time-frequency dictionaries," *IEEE Transactions on Signal Processing*, vol. 41, pp. 3397–3415, 1993.

[42] S. Qian and D. Chen, "Decomposition of the Wigner distribution and time-frequency distribution series," *IEEE Transactions on Signal Processing*, vol. 42, p. 2836–2842, 1994.

[43] A. Papandreou-Suppappola and S. Suppappola, "Adaptive time-frequency representations for multiple structures," in *IEEE Workshop on Statistical Signal Array Processing*, p. 579–583, 2000.

[44] S. M. Kay, *Fundamentals of Statistical Signal Processing, Volume I: Esimation Theory*. Prentice-Hall, 1993.

[45] F. Hlawatsch and G. F. B. Bartels, "Linear and qaudratic time-frequency signal representations," *IEEE Signal Processing Magazine*, vol. 9, pp. 21–67, 1992.

[46] A. Papandreou-Suppappola, "Generalized time-shift covariant quadratic time-frequency representations with arbitrary group delays," in *Asilomar inproceedings on Signals, Systems and Computers*, p. 553–557, 1995.

[47] M. R. McClure and L. Carin, "Matching pursuits with a wave-based dictionary," *IEEE Transacitons on Signal Processing*, vol. 45, p. 2912–2927, 1997.

[48] A. Bultan, "A four-parameter atomic decomposition of chirplets," *IEEE Transacitons on Signal Processing*, vol. 47, pp. 731–745, 1999.

[49] C. Fraley and A. E. Raftery, "Model-based clustering, discriminant analysis, and density estimation," *Journal of the American Statistical Association*, vol. 97, pp. 611–631, 2002.

[50] C. M. Bishop, *Pattern recognition and machine learning*. springer, 2006.

[51] D. Reynolds, "Gaussian mixture models," *Encyclopedia of Biometrics*, pp. 827–832, 2015.

[52] M. R. Gupta and Y. Chen, *Theory and Use of the EM Algorithm*. Now Foundations and Trends, 2011.

[53] T. A. C. M. Claasen and W. F. G. Mecklenbr auker, "The Wigner distribution—a tool for time-frequency signal analysis, part II, discrete-time signals," *Philips Journal of Research*, vol. 35, p. 276–300, 1980.

[54] M. S. Richman, T. W. Parks, and R. G. Shenoy, "Discrete-time, discrete-frequency time-frequency analysis," *IEEE Transactions on Signal Processing*, vol. 46, p. 1517–1527, 1998.

[55] C. Richard, "Linear redundancy of information carried by the discrete Wigner distribution," *IEEE Transactions on Signal Processing*, vol. 49, pp. 2536–2544, 2001.

[56] E. Chassande-Mottin and A. Pai, "Discrete time and frequency Wigner–Ville distribution: Moyal's formula and aliasing," *IEEE Signal Processing Letters*, vol. 12, pp. 508–511, 2005.

[57] J. O. Toole, M. Mesbah, and B. Boashash, "A new discrete analytic signal for reducing aliasing in the discrete Wigner-Ville distribution," *IEEE Transactions on Signal Processing*, vol. 56, pp. 5427–5434, 2008.

APPENDIX A

UNITARITY PROPERTY OF THE DISCRETE WIGNER DISTRIBUTION

The unitarity property or Moyal's formula shows that the Wigner distribution (WD) preserves the inner product between two signals $x(t)$ and $y(t)$. Specifically,

$$\int_{-\infty}^{\infty}\int_{-\infty}^{\infty} W_x(t,f)\, W_y^*(t,f)dt\, df = \left|\int_{-\infty}^{\infty} x(t)\, y^*(t)\, dt\right|^2 \tag{A.1}$$

where the WD of $x(t)$ is defined as

$$W_x(t,f) = \int_{-\infty}^{\infty} x\left(t+\frac{\tau}{2}\right)\, x^*\left(t-\frac{\tau}{2}\right)\, e^{-j2\pi\tau f}\, d\tau\,.$$

For implementation, the signal samples $x[n] = x(nT_s)$ are obtained using sampling period T_s. Note, however, that a discrete WD that satisfies all the signal properties of the continuous WD is not possible [53, 54, 55, 56, 57]. In order to preserve inner products as in Equation (A.1), we use the discrete WD (DWD) for complex or analytic signals $x[n]$ provided in [55]. The DWD is defined as

$$W_x[n,k] = \sum_{m=0}^{N-1} x[n+m]\, x^*[n-m]\, \exp(-j2\pi k\, m/N)\,,$$

$$n = 0,\ldots,N-1,\;\; k = 0,\ldots,N-1\,, \tag{A.2}$$

where $0 \leqslant n-m \leqslant N-1$ and $0 \leqslant n+m \leqslant N-1$. The corresponding unitarity property for the DWD is given by

$$\Lambda = \frac{1}{N}\sum_{n=0}^{N-1}\sum_{k=0}^{N-1} W_x[n,k]\, W_y[n,k] = \left|\sum_{n=0}^{N-1} x[n]\, y^*[n]\right|^2\,. \tag{A.3}$$

The proof of unitarity in Equation (A.3) is as follows.

We first substitute the DWD from Equation (A.2) on the left-hand side of Equation (A.3).

Specifically,

$$\Lambda = \frac{1}{N}\sum_{n=0}^{N-1}\sum_{k=0}^{N-1} W_x[n,k]\, W_y[n,k]$$

$$= \frac{1}{N}\sum_{n=0}^{N-1}\sum_{k=0}^{N-1}\left(\sum_{m=0}^{N-1} x[n+m]\, x^*[n-m]\, e^{-j2\pi k\, m/N}\right)\times$$

$$\left(\sum_{\ell=0}^{N-1} y[n+\ell]\, y^*[n-\ell]\, e^{-j2\pi k\, \ell/N}\right)^*$$

$$= \sum_{n=0}^{N-1}\sum_{m=0}^{N-1}\sum_{\ell=0}^{N-1} x[n+m]\, x^*[n-m]\, y^*[n+\ell]\, y[n-\ell] \sum_{k=0}^{N-1} e^{j2\pi k(\ell-m)/N} \quad \text{(A.4)}$$

Using the following two equations

$$\sum_{k=0}^{N-1} e^{j2\pi k(\ell-m)/N} = N\,\delta[\ell-m]\,,$$

and

$$\sum_{n=0}^{N-1} r[n]\,\delta[n-m] = r[m],\ \ 0 \leqslant m \leqslant N-1\,,$$

then Equation (A.4) can be simplified to

$$\Lambda = \sum_{n=0}^{N-1}\sum_{m=0}^{N-1}\sum_{\ell=0}^{N-1} x[n+m]\ x^*[n-m]\ y^*[n+\ell]\ y[n-\ell]$$

Letting $i = n+m$ and $l = n-m$, then $n = \frac{i+l}{2}$ and $m = \frac{i-l}{2}$, resulting in

$$\Lambda = \sum_{i=0}^{N-1}\sum_{l=0}^{N-1} x[\,i\,]y^*[\,i\,]\,y[\,l\,]\,x^*[\,l\,]$$

$$= \left(\sum_{i=0}^{N-1} x[\,i\,]\ y^*[\,i\,]\right)\left(\sum_{l=0}^{N-1} x[\,l\,]\,y^*[\,l\,]\right)^*$$

$$= \left|\sum_{n=0}^{N-1} x[n]\, y^*[n]\right|^2$$

which is the equation on the right-hand side of Equation (A.3).